学　位　論　文

Development of Exacerbation Prediction Model for Patients with Refractory Asthma Based on Peak Flow Monitoring data

(ピークフローモニタリングデータに基づいた難治性喘息患者における

増悪予測モデルの開発)

２０２５年3月

北　海　道　大　学

楊　　一　馳　（ヤン　イチ）

Yichi Yang

学　位　論　文

Development of Exacerbation Prediction Model for Patients with Refractory Asthma Based on Peak Flow Monitoring data

(ピークフローモニタリングデータに基づいた難治性喘息患者における

増悪予測モデルの開発)

２０２５年3月

北　海　道　大　学

楊　　一　馳　（ヤン　イチ）

Yichi Yang

Contents

List of publications and presentations

Part of the research has been published as listed below:

1. Yang Y, Kimura H, Yokota I, Makita H, Takimoto-Sato M, Matsumoto-Sasaki M, Matsumoto M, Oguma A, Abe Y, Takei N, Goudarzi H, Shimizu K, Suzuki M, Nishimura M, Konno S, Hi-CARAT investigators. Applicable predictive factors extracted from peak flow trajectory for the prediction of asthma exacerbation. Ann Allergy Asthma Immunol. 2023 Nov 24:S1081-1206(23)01464-3.

Abstract

【Introduction】

Asthma is a common respiratory disease, asthma-related deaths have barely decreased despite the increase in asthma care. It remains a prevalent respiratory condition with substantial morbidity and mortality, particularly among patients with severe or refractory forms who experience persistent symptoms and are at high risk of acute exacerbations. Though type 2 inflammation is considered the predominant pathology in asthma exacerbation, non-type 2 inflammation also exists, particularly in patients with refractory asthma who do not respond well to corticosteroid treatment. The heterogeneity in asthma pathology complicates efforts to prevent exacerbations.

Chapter 1 Real-time exacerbation prediction model

【Introduction】

Real-time asthma exacerbation prediction and upcoming acute asthma attack detection are essential for patients with severe asthma. Among several potential predictors, peak expiratory flow (PEF) exhibits a potential for use in long-term asthma self-monitoring. However, the method for processing PEF calculations remains to be clarified. We propose two novel PEF-based metrics, the delta moving average (ΔMA) and the delta percentage predicted PEF moving average (%ΔMA), to facilitate real-time exacerbation prediction.

【Materials and Methods】

PEF records were collected from the Hokkaido-based Investigative Cohort Analysis for Refractory Asthma (Hi-CARAT). Hi-CARAT is a multicenter observation study that included adult patients with severe asthma with or without smoking history in Hokkaido Prefecture, Japan, from which 127 patients with severe asthma and 73,503 PEF observations were obtained. Previously proposed exacerbation predictors, including the decreasing trend of PEF, percentage predicted PEF, percentage best PEF, the highest PEF over the lowest PEF within specific periods, and PEF coefficient of variation, as well as a novel indicator ΔMA, defined as the difference between 14-day and 3-day average PEF values along with ΔMA adjusted for PEF reference (%ΔMA), were verified using the Hi-CARAT. Receiver operating characteristic curves for all predictors were drawn and the corresponding areas under the curve (AUCs) were computed. Regression analysis for ΔMA and %ΔMA were conducted.

【Results】

The most outstanding performance was demonstrated by ΔMA and %ΔMA, with AUC values of 0.659 and 0.665 in the univariate model, respectively. Incorporating ΔMA and %ΔMA into multivariate models further improved the AUCs to 0.710 and 0.707. When multivariate models incorporated with random intercepts for individual participants, the AUC for ΔMA and %ΔMA soared to 0.907 and 0.919, respectively. Several possible cutoff values for ΔMA and %ΔMA were proposed.

【Discussion】

The ΔMA and %ΔMA are valuable indicators that should be considered when deriving predictors from the PEF trajectory for monitoring exacerbations in patients with severe asthma. Our findings also suggested that using a single PEF-based predictor may not be sufficient, emphasizing the need for multivariate approaches. While our model offers a promising approach to real-time exacerbation prediction, limitations include potential measurement errors, reliance on patient compliance, and a lack of precise timing for bronchodilator use in the Hi-CARAT study. Future research should focus on combining subjective and objective measures for a more comprehensive predictive model. Despite these limitations, our study provides valuable insights into leveraging PEF trajectories for predicting asthma exacerbations in severe cases.

Chapter 2 Patients' categorization and vulnerability prediction model

【Introduction】

Besides the real-time prediction, the PEF monitoring data can also be used to evaluate the patient vulnerability to exacerbation. We developed a modified latent class joint model (LCJM) that categorizes asthma patients based on whether their PEF trajectories are responsive to upcoming exacerbations, allowing individualized assessment of vulnerability.

【Materials and Methods】

We developed a modified LCJM with the association term (ASC) shared between the longitudinal and time-to-event submodels to analyze longitudinal and time-to-event data, specifically to capture heterogeneity in asthma patients' PEF trajectories. The longitudinal submodel utilized an additive framework to model PEF measurements, while the time-to-event submodel employed a parametric survival model with a Weibull baseline hazard

function. Parameter estimation was performed using a two-step approach, leveraging the Expectation-Maximization algorithm to account for unobserved latent categories. The logistic submodel was used to predict the probability of latent class membership. To validate the model, we conducted a simulation study with 100 participants, each traced over five periods. Two censoring scenarios were evaluated: no censoring and right censoring at the time point k=10. The model's performance was assessed through parameter estimation accuracy, latent class discrimination using the c-index, and Kaplan-Meier survival curve.

【Results】

The simulation studies validated the model's accuracy and robustness. Parameter estimation results were consistent across no censoring and right censoring scenarios, with low bias and stable average sample standard error and empirical standard error values. The LCJM yielded superior Gönen and Heller c-index scores (no censoring scenario: 0.611; right censoring scenario: 0.620, targeting participants predicted to be recruited from category 0. no censoring scenario: 0.663; right censoring scenario: 0.674, targeting participants predicted to be recruited from category 1) compared to conventional time-to-event model (no censoring scenario: 0.544; right censoring scenario: 0.550, assuming all participants are recruited from the category 0) and joint models (no censoring scenario: 0.654; right censoring scenario: 0.652, assuming all participants are recruited from the category 1). Kaplan-Meier survival plot showed that the model accurately classified participants into categories. The category discrimination c-index was 0.956 (no censoring scenario) and 0.955 (right censoring scenario), indicating that the model reliably identified latent classes.

【Discussion】

The model we proposed has proven to be a potential choice for estimating the vulnerability towards exacerbation in patients with asthma based on the simulation study. However, the model has limitations, including potential oversimplification of participant categories and possible misspecification of the survival submodel. Future research should explore extending the model to a multinomial framework and incorporating individual frailty effects. Implementing this model on real-world datasets, such as the Hi-CARAT dataset, is also a key focus of our next study step. Despite these limitations, our findings offer valuable insights for enhancing PEF monitoring in severe asthma management.

【Conclusion】

We have confirmed that PEF monitoring data can be effectively used for real-time exacerbation prediction in patients with severe asthma. Additionally, we extended the LCJM framework to incorporate heterogenous PEF trajectories within patients with severe asthma assuming a part of them may present segmented linear structure in their PEF trajectories. We hope the results of this study help in the construction of a clinically applicable exacerbation prediction model in the future.

List of Abbreviations

%bestPEF – Percentage best PEF

%ΔMA – Delta percentage predicted PEF moving average

%predPEF – Percentage predicted PEF

ASC – Association term shared between longitudinal and time-to-event submodel

ASE – Average sample standard error

AUC – Area under the curve

CV – Coefficient of variation

EM – Expectation-Maximization

ESE – Empirical standard error

FeNO – Fractional exhaled nitric oxide

Hi-CARAT – Hokkaido-based Investigative Cohort Analysis for Refractory Asthma

IgE – Immunoglobulin E

IgM – Immunoglobulin M

IL – Interleukin

L-BFGS-B – Limited-memory Broyden–Fletcher–Goldfarb–Shanno with Box constraints

LCJM – Latent class joint model

ΔMA – Delta moving average

Min/Max – The highest PEF over the lowest PEF within specific periods

NO_2 – Nitrogen dioxide

O_3 – Ozone

PBE – Peripheral blood eosinophils

pDCs – Plasmacytoid dendritic cells

PEF – Peak expiratory flow

ROC – Receiver operating characteristic

SD – Standard deviation

SO_2 – Sulphur dioxide

SPM – Suspended particulate matter

Introduction

Asthma, a prevalent respiratory condition, is characterized by bronchial narrowing, which manifests as wheezing, excessive mucus secretion, and difficulty breathing (Thomas et al., 2010). Despite advancements in asthma management, the global mortality rate associated with the disease has shown minimal reduction over time (Ebmeier et al., 2017). A subset of asthma patients, particularly those classified as severe or refractory, remains resistant to treatment and continues to experience poorly controlled symptoms, leaving them vulnerable to potentially life-threatening acute exacerbations (Lommatzsch and Virchow, 2014; Schoettler and Strek, 2020). Asthma surveillance and exacerbation prediction for patients with severe asthma are topics of great interest to researchers.

The mechanisms underlying asthma exacerbation have been explored in numerous studies. Inflammatory responses, especially type 2 inflammation, are considered key contributors to asthma exacerbations. It is reported that the type 2 inflammation was observed in 84% of adult patients with asthma visiting clinics (Jackson et al., 2018). The type 2 inflammation is driven by the overexpression of interleukin (IL) -4, IL-5 and IL-13 which play an essential role in the asthma pathophysiology (Gallagher et al., 2021; Hammad and Lambrecht, 2021). The structures of IL-4 and IL13 are similar and they are both involved in the class switching from immunoglobulin M (IgM) to immunoglobulin E (IgE) (Li et al., 2014; Gour and Wills-Karp, 2015). IgE can occupy the membrane receptors on plasmacytoid dendritic cells (pDCs), enabling the cross-linking of IgE receptors by allergen, and increasing the risk of asthma exacerbations (Castillo et al., 2017). Meanwhile, the IL-5 regulates the conduction and maturation of eosinophils (Lopez et al., 1986). Overexpression of these ILs is associated with increased eosinophil counts in the blood, bronchial tissue, and sputum, as well as elevated levels of fractional exhaled nitric oxide (FeNO) (Pizzichini et al., 1998; Brightling et al., 2000; Siva et al., 2007; Garudadri and Woodruff, 2018; Barnes, 2019). Although the role of eosinophils in asthma is still debated, clinical studies using IL-5 antibodies, such as mepolizumab, have shown a reduction in blood and sputum eosinophil counts (Flood-Page et al., 2007; Foster et al., 2008). Nevertheless, not all the patients with asthma exhibit type 2 airway inflammation (Duvall et al., 2019). Non-type 2 inflammation, particularly in patients with refractory asthma who do not respond well to corticosteroid treatment, warrants attention. The biomarkers for non-type 2 asthma remain controversial and the heterogeneity in asthma pathology complicates efforts to prevent exacerbations (Hudey et al., 2020).

Efforts to prevent exacerbations can be categorized into two main approaches: 1) real-time prediction of exacerbations to enable timely intervention and early medication, and 2) assessment of patient vulnerability to identify those at higher risk of exacerbation. We

aim to propose novel PEF-based approaches to address the current research gap. In the first part of this study, we propose a novel, easily accessible PEF statistic for real-time exacerbation prediction, namely the delta moving average (ΔMA) and the delta percentage predicted PEF moving average (%ΔMA). We developed univariate and multivariate logistic models to evaluate their predictive performance in identifying impending exacerbations, enabling individualized intervention for medical visits or medication administration. In the second part, we developed a modified latent class joint model (LCJM) to categorize patients with asthma into two groups: those whose PEF trajectories remain stable and those whose PEF trajectories decline prior to exacerbation. By capturing population heterogeneity, we assessed the vulnerability to exacerbations in each group.

Chapter 1 Real-time Exacerbation Prediction Model

Introduction

Previous studies have identified various predictive factors for asthma exacerbation, including weather conditions, air pollution, exhaled chemical substances, and inflammatory biomarkers (Bime et al., 2012; Hayata et al., 2013; Kimura et al., 2018). For example, a decrease in temperature has been associated with airway hyper-responsiveness and narrowing (Kaminsky et al., 2000; Buckley and Richardson, 2012), with a systematic review further confirming that temperature drops serve as a risk factor for asthma exacerbations (Cong et al., 2017). The adverse effects of air pollution on asthma outcomes have also been extensively studied. Specifically, exposure to ozone (O_3), sulfur dioxide (SO_2), nitrogen dioxide (NO_2), and suspended particulate matter (SPM) at concentrations exceeding legal thresholds has been linked to a heightened risk of exacerbations (Tiotiu et al., 2020). Furthermore, FeNO, a biomarker for eosinophilic inflammation, has been proposed as a predictor of future asthma exacerbations (Pijnenburg, 2019; Murugesan et al., 2023). While these findings offer valuable insights for managing exacerbations, many of the predictors mentioned above are not easily accessible for self-monitoring by patients. For instance, blood tests and exhaled biomarker analyses require laboratory settings and cannot be conducted at home. Although weather and air pollution data are readily available to patients without the assistance of healthcare providers, these indicators reflect only external environmental conditions and not the patient's internal health status. Self-monitoring tools like the Asthma Control Questionnaire (Juniper et al., 1999), Asthma Quality of Life Questionnaire (Juniper et al., 1992) and Asthma Symptom Utility Index (Revicki et al., 1998) have been suggested but are limited by patient subjectivity and the time required for completion.

Peak expiratory flow (PEF), an objective measure of airway obstruction, has been widely used for asthma monitoring in clinical practice (Antalffy et al., 2020). The increasing availability of portable PEF meters has enabled patients to measure PEF at home, facilitating self-monitoring and better asthma control (Sun et al., 2018). PEF is also a promising real-time predictor of asthma exacerbations, offering the potential to forecast exacerbation likelihood based on PEF trajectories. However, the use of PEF as a predictor remains underexplored. Prior research has linked the percentage predicted PEF (%predPEF) to airway obstruction (Frey et al., 2005). A previous study suggested that PEF statistics, such as the mean, coefficient of variation (CV), and autocorrelation, could help predict loss of asthma control. Among these, CV has been identified as a potential predictor of asthma control loss (Thamrin et al., 2010). Additionally, studies suggest that

the highest PEF over the lowest PEF within specific periods (Min/Max) is associated with asthma symptoms and exacerbation (Hayata et al., 2013; Honkoop et al., 2013). Reductions in PEF have also been reported as indicators of impending asthma attacks (Thamrin et al., 2011). Despite these findings, the computation of PEF statistics, such as variation and decreasing trends, imposes a considerable calculation burden, complicating their clinical application. In this section, we introduce a novel predictor derived from PEF monitoring, assess its discriminative power, and compare it with conventional PEF-based predictors.

Materials and Methods

Study materials

The PEF data used in this study were obtained from the Hokkaido-based Investigative Cohort Analysis for Refractory Asthma (Hi-CARAT, UMIN ID: 000003254). Hi-CARAT is a multicenter observational study conducted in Hokkaido Prefecture, Japan, involving adult patients with severe asthma, regardless of their smoking history. This study received ethical approval from the ethics committee of Hokkaido University Hospital (approval number, 009-0205), and all participants provided written informed consent. It was also registered in the University Hospital Medical Information Network Clinical Trials Registry system. The registration information can be checked on the following website https://upload.umin.ac.jp/cgi-open-bin/ctr/ctr_view.cgi?recptno=R000003917.

Participants were recruited from Hokkaido University Hospital and 29 of its affiliated clinics and hospitals (Kimura et al., 2017). The inclusion criteria for patients with severe asthma were based on the American Thoracic Society criteria for refractory asthma 2000 version (Wenzel et al., 2000), with slight modifications. Two additional criteria were included: 1) a severe asthma diagnosis with one or both major criteria and two minor criteria being met and 2) patients receiving medication and in a well-controlled condition were asked if they needed urgent medical care visits and short-acting bronchodilators or experienced episodic deterioration of symptoms when the dose of the current medication was reduced within the last year (Kimura et al., 2018). The cohort study was conducted between February 2010 and March 2019, with airway function monitoring taking place from February 2010 to September 2015. This analysis included airway function data from 127 patients with severe asthma collected between 2010 and 2015, with follow-up durations ranging from 2 to 42 months. Due to variable enrollment times, the first participant completed airway function monitoring on April 23, 2010, while the last participant finished on September 11, 2015.

PEF measurements were collected using the Piko-1 (nSpire Health, Inc., USA), an electronic peak flow meter validated in earlier studies (Fonseca et al., 2005; Dal Negro et al., 2007). Participants were instructed to measure their PEF twice daily (morning and evening) over a 30-day period every 3 months, resulting in a total of 73,503 recorded PEF values. The initial two months of the study were designated as a practice period to ensure participants accurately performed the PEF measurement technique. Data were electronically processed and analyzed after each 30-day session, and outlier identification was conducted independently by three physicians. Data were excluded if judged as outliers by at least two physicians. The PEF trajectories and asthma exacerbation periods were documented. In Hi-CARAT, asthma exacerbation was defined as the use of systemic

corticosteroids for more than three days and/or severe exacerbations necessitating hospitalization (Kimura et al., 2018). A total of 467 exacerbations were recorded. For example, Figure 1 depicts a portion of the PEF trajectory of patient number 98, shown in a time-series format.

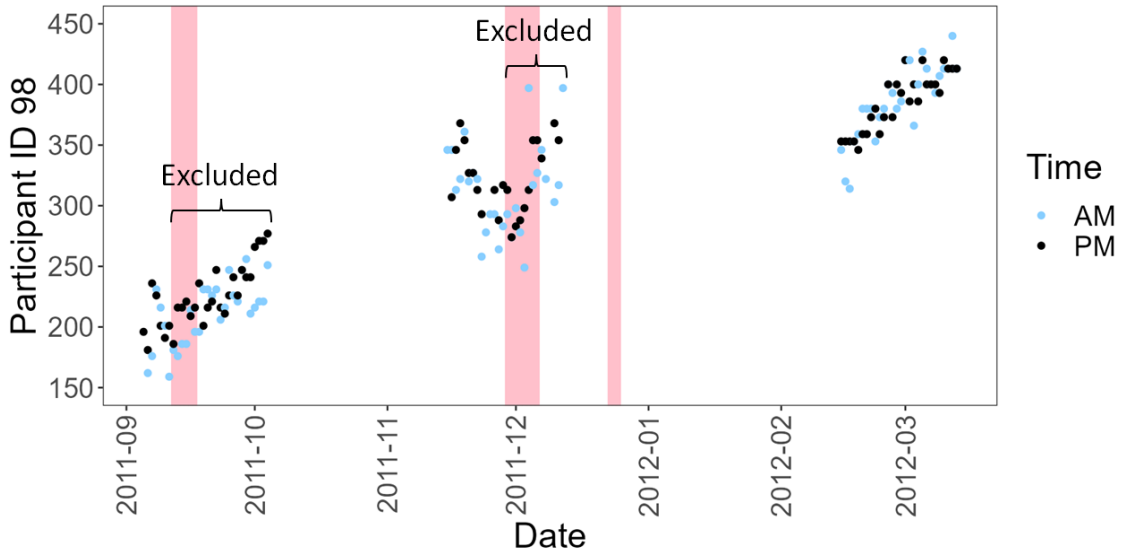

Figure 1. Example of data and exclusion criteria

A segment of PEF measurements from participant number 98, recorded between September 2011 and April 2012, is shown. The vertical axis represents PEF values (L/min), while the horizontal axis indicates the recording dates. Pink-shaded regions correspond to periods of exacerbation.

The vertical axis represents PEF values (L/min), while the horizontal axis corresponds to the calendar date. Measurements were typically taken every 3 months, with an average 2-month gap between sessions. Pink-shaded areas indicate exacerbation periods during which symptom relief medication was administered. Light blue points denote daytime measurements, whereas black points indicate nighttime readings. To minimize interference from medication-induced PEF improvement, data collected during or immediately after exacerbation periods were excluded from the analysis for each measurement cycle.

Statistical analyses

Key metrics derived from PEF trajectories were calculated for each calendar date, including the PEF slope, standard deviation (SD), maximum and minimum PEF values, as well as mean PEF values over 3-, 7-, and 14-day intervals. The PEF slope, representing the time coefficient in a univariate linear regression model, was calculated by setting PEF as the dependent variable and time as the independent variable. This metric reflects the

evolving trend of PEF over time, where a positive slope indicates an increase in PEF, and a zero or negative slope indicates stability or decline. Given the twice-daily PEF measurement rule, time was expressed in half-day units. The CV was computed as:

$$\mathrm{CV} = \frac{\mathrm{SD}}{\mathrm{Mean}},$$

that is, SD divided by the means within a specified period. It illustrates the variability of the PEF trajectory regardless of the mean PEF value. The Min/Max was calculated using the following equation:

$$\frac{\mathrm{Min}}{\mathrm{Max}} = \frac{\text{Period minimum PEF}}{\text{Period maximum PEF}},$$

serving as another indicator of PEF variability.

$$\%\mathrm{predPEF} = \frac{\mathrm{PEF}}{\text{PEF ref}}.$$

The %predPEF was determined by dividing the measured PEF by a reference PEF value calculated using sex, height, and age, based on a recently developed equation for East Asian populations:

For males:

$$\text{PEF ref} = exp[-7.0972 + 1.6544 \times ln(h) + 0.2314 \times ln(y) + \text{spline}],$$

For females

$$\text{PEF ref} = exp[-6.63189 + 1.61459 \times ln(h) + 0.08976 \times ln(y) + \text{spline}],$$

where h denotes the participant's height in cm, and the y represents the age in years. The spline is the age-specific contribution of the spline function (Jian et al., 2017). For participants over 81 years old (n=2), where spline values were unavailable, the spline value for 81 years was applied.

$$\%\mathrm{bestPEF} = \frac{\mathrm{PEF}}{\text{personal best PEF}}.$$

Other than setting the PEF reference as the denominator, we also calculated the percentage best PEF (%bestPEF) dividing PEF by the patients best recorded PEF. In addition to these indicators introduced in previous studies, a novel predictor, ΔMA, was introduced to capture both the trend and variability of smoothed PEF values. It was calculated as:

$$\Delta\mathrm{MA} = \text{14 day PEF average} - \text{3 day PEF average}.$$

This simple calculation, requiring only the mean and difference in PEF, makes it suitable for self-monitoring. The percentage change in ΔMA (%ΔMA) was computed to assess whether using %predPEF instead of PEF improved predictive performance:

$$\%\Delta\mathrm{MA} = \text{14 day \%predPEF average} - \text{3 day \%predPEF average}.$$

To evaluate the predictive power of PEF slope, CV, Min/Max, %predPEF, %bestPEF, ΔMA, and %ΔMA, receiver operating characteristic (ROC) curves were generated, with sensitivity plotted against 1 − specificity. The area under the curve (AUC) was used to compare the discriminative performance of each predictor. Prediction curves with confidence intervals were also created to illustrate how exacerbation risk changes with ΔMA or %ΔMA.

Logistic regression was employed to predict real-time asthma exacerbations with a dichotomous outcome (whether an exacerbation would occur the following day). Two univariate logistic models were constructed, using ΔMA and %ΔMA as independent variables, respectively. Model calibration was assessed via the Hosmer–Lemeshow test, and subgroup analyses were performed based on age, sex, atopy status, and smoking status (Hosmer and Lemeshow, 2013). Multivariate logistic models were developed by incorporating covariates: sex, body mass index, waist circumference, serum IgE levels, peripheral blood eosinophils (PBE), FeNO, atopy status, smoking status, and exposure to air pollutants (nitrogen dioxide, sulfur dioxide, and suspended particulate matter). To account for individual variations not captured by these covariates, To account for individual variations beyond these covariates, mixed-effects models were constructed for both ΔMA and %ΔMA. All statistical analyses were conducted using R software (R Development Core Team, 2019).

Results

Table 1. Patient characteristics (N = 127)

Characteristics	N (%) / Mean ± standard deviation
Male	51 (40.2%)
Age, y	58.0 ± 13.1
Age at onset of asthma, year	38.2 ± 17.7
Body mass index, kg/m^2	25.6 ± 5.5
Atopy positivity	81 (63.8%)
Smoking status	N (%) / Median (interquartile range)
Current	13 (10.2%)
Previous	62 (48.8%)
Never	52 (40.9%)
Pack-years	5.0 (0, 22.7)
Peripheral blood/serum	Geometric mean (log10 standard deviation)
Eosinophils, cells/μl	203.4 (0.5)
Neutrophils, cells/μl	4,554.4 (0.17)
Corticosteroid use	N (%) / Mean ± standard deviation
Inhaled corticosteroid dose, μg	1649 ± 574
Oral corticosteroid use	45 (35.4%)
Pulmonary function	Mean ± standard deviation / median (interquartile range)
FEV_1 % predicted (prebronchodilator)	82.8 ± 19.4
FEV_1/FVC	67.1 ± 13.0
PEF, L/min	307.0 (247.0, 397.0)
%prePEF	78.6% (61.7%, 96.4%)
Number of exacerbation onsets	1 (0, 4)

Overall, 127 patients with severe asthma were included. FEV1 measurements were obtained during hospital stays at Hokkaido University Hospital, while PEF data were collected through longitudinal self-monitoring by the participants.

Table 1 summarizes the baseline characteristics of the study participants. Categorical variables, such as the number of male participants, those with a positive atopy test result, participants with a history of smoking, and individuals receiving oral corticosteroids, are presented as counts and percentages. Eosinophil and neutrophil counts are reported as geometric means with log10 SD, while continuous variables are expressed as mean ± SD or median (interquartile range). The participants were all adults, with an average age of 58 years. Among the 127 individuals, 51 were male, and 76 were female. A “never-smoker” was defined as someone with a Brinkman Index of 0, indicating no history of smoking. By the end of the study, 75 participants had a history of smoking, and 45 had been treated

with oral corticosteroids. Blood eosinophil counts in this cohort were relatively low, with a geometric mean of 203.4 cells/μl. The median rare PEF value and %predPEF were 307.0 L/min and 78.6%, respectively.

To evaluate the real-time predictive power of asthma exacerbations, ROC curves were generated for several previously proposed indicators, including PEF slope, %predPEF, %bestPEF, Min/Max, and CV.

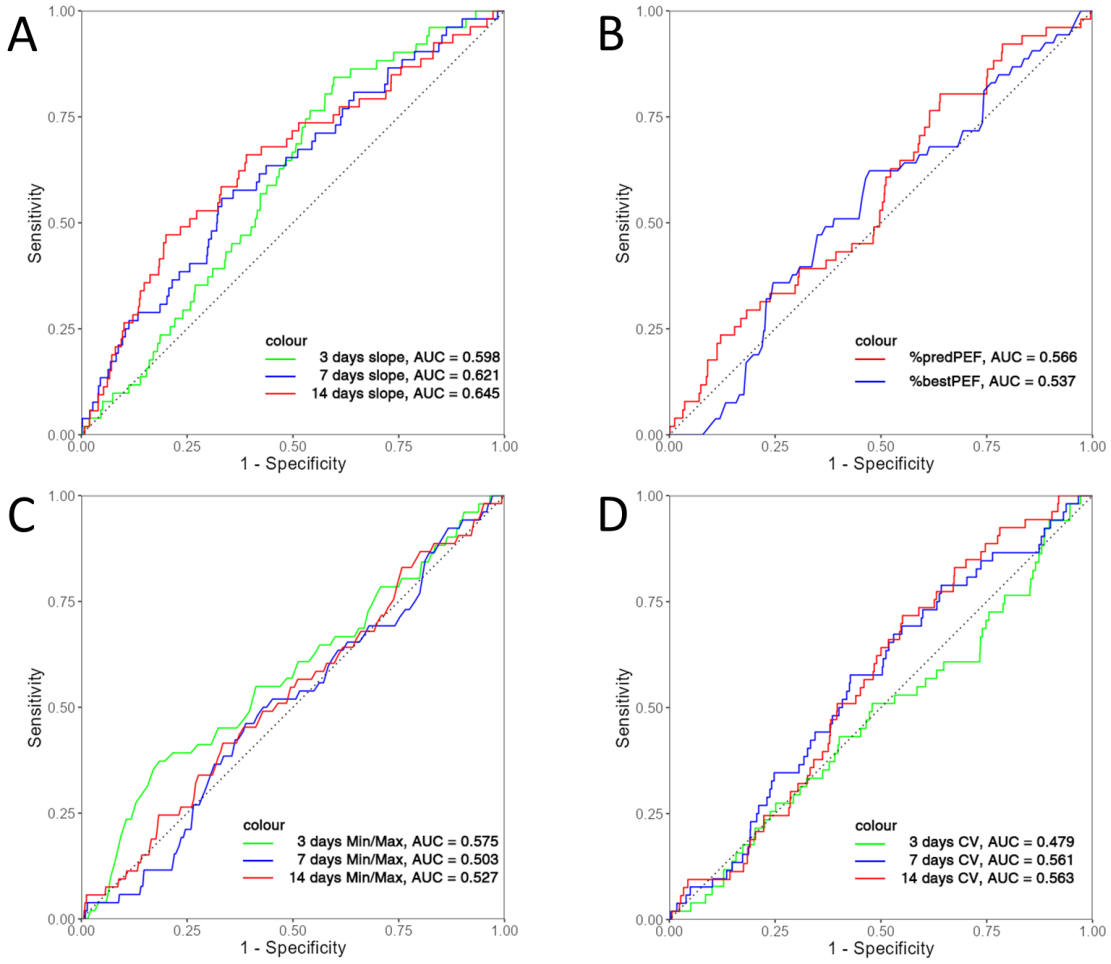

Figure 2. ROCs for slope, %predPEF, %bestPEF, Min/Max, and CV

Panel A, C, and D depict the ROC curves for variables calculated over 3, 7, and 14 days, represented by green, blue and red lines, respectively. The discriminative performance, expressed as the AUC, is provided in the graph legends. Among these, the 14-day PEF slope demonstrated the highest discriminative ability, with an AUC of 0.645.

Figure 2 displays the results, with sensitivity plotted on the y-axis and 1 − specificity on the x-axis across all panels. Panel A illustrates the ROC curves for the PEF slope calculated over 3, 7, and 14 days, differentiated by colors. The 14-day slope demonstrated

the highest discriminative performance, with its AUC exceeding those for shorter time periods. Panel B shows the ROC curves for %predPEF (AUC = 0.566) and %bestPEF (AUC = 0.537). Panel C presents the ROC curves for Min/Max across the same time intervals, with poor performance regardless of the interval. Similarly, Panel D shows the ROC curves for CV over 3, 7, and 14 days, with low AUC values of 0.479, 0.561, and 0.563, respectively. These findings highlight those indicators reflecting the trend, such as slope, generally achieved higher AUCs compared to variability-based metrics like CV.

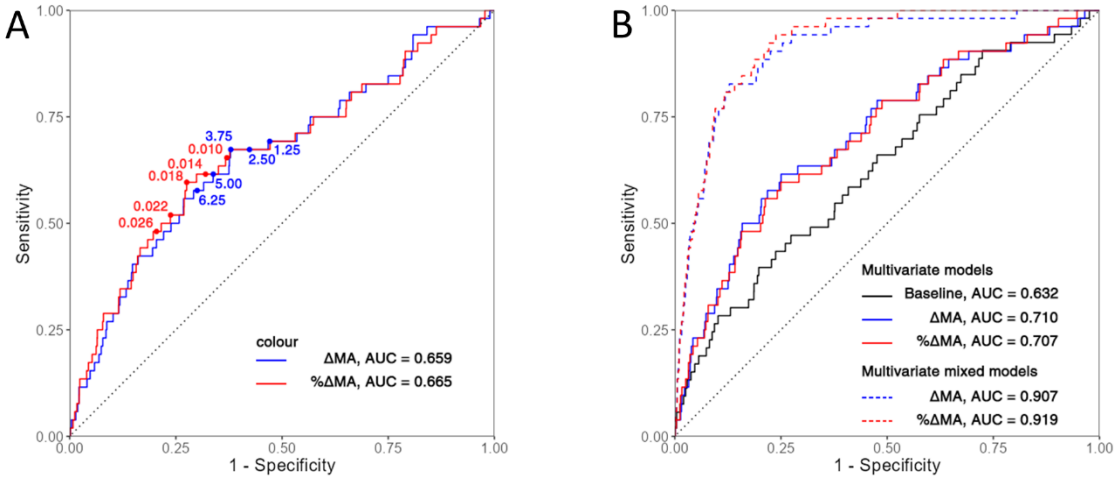

Figure 3. ROC for ΔMA and %ΔMA

ΔMA and %ΔMA demonstrated the highest discriminative performance among all predictors. This superior performance remained consistent in the context of multivariate regression. When random intercepts were incorporated, the AUC values for ΔMA and %ΔMA increased significantly to 0.907 and 0.919, respectively.

Figure 3 presents the ROC curves for the novel indicators, ΔMA and %ΔMA. Among all metrics, %ΔMA exhibited the best performance with an AUC of 0.665, slightly higher than the AUC of ΔMA at 0.659. Importantly, the Youden index was not used to optimize cutoff values, as its assumption of equal sensitivity and specificity is not appropriate for exacerbation prediction (Ruopp et al., 2008). Treating a well-controlled patient unnecessarily is not equivalent to overlooking a severe asthma patient at risk of exacerbation. Instead, five reference cutoff values were proposed for ΔMA and %ΔMA, marked on the ROC curves in Figure 3A. These cutoffs aim to guide the timing of medical interventions for patients with severe asthma. Table 2 presents the sensitivity and specificity for each cutoff, showing that as the cutoff value increases, sensitivity declines, while specificity improves.

Table 2. Discriminant performance of potential cutoff value

	Cutoff	Sensitivity	Specificity
ΔMA	1.250	0.692	0.529
	2.500	0.673	0.577
	3.750	0.673	0.621
	5.000	0.615	0.662
	6.250	0.577	0.700
%ΔMA	0.010	0.654	0.630
	0.014	0.615	0.680
	0.018	0.596	0.724
	0.022	0.519	0.762
	0.026	0.481	0.796

Serial potential cutoff values of PEF ΔMA and %ΔMA along with their corresponding discriminative performance metrics, including sensitivity and specificity are listed. As the cutoff value increases, sensitivity decreases, while specificity correspondingly increases.

In multivariate models incorporating demographic, clinical, and environmental factors—such as sex, BMI, waist circumference, serum IgE levels, PBE, FeNO, atopy status, smoking history, and air pollutants (NO_2, SO_2, and SPM)—the AUCs for ΔMA and %ΔMA improved to 0.710 and 0.707, respectively. A baseline AUC of 0.632 was calculated using only these covariates without ΔMA or %ΔMA, indicating that ΔMA and %ΔMA provided additional discriminative power of 0.078 and 0.075, respectively. By substituting ΔMA or %ΔMA with other PEF indicators (e.g., the 14-day slope or 3-day Min/Max), lower AUC values were observed, such as 0.641 for the 14-day slope and 0.666 for 3-day Min/Max. When these multivariate models were advanced to mixed-effect models, accounting for individual variability as random effects, the AUCs for ΔMA and %ΔMA increased significantly to 0.907 and 0.919, respectively.

Table 3. Model calibration and subgroup analysis

	Participants		AUC		Hosmer–Lemeshow p-value	
	N	%	ΔMA	%ΔMA	ΔMA	%ΔMA
All	127	100%	0.659	0.665	0.654	0.483
Age (y)						
≥65	47	0.370	0.632	0.643	0.696	0.566
< 65	80	0.630	0.670	0.674	0.419	0.518
Sex						
Male	51	0.402	0.599	0.597	0.391	0.445
Female	76	0.598	0.686	0.687	0.134	0.125
Atopy						
Positive	81	0.638	0.663	0.664	0.737	0.630
Negative	46	0.362	0.657	0.666	0.026*	0.017*
Smoking						

Yes	75	0.591	0.604	0.611	0.542	0.501
No	52	0.409	0.757	0.754	0.034*	0.049*

A significance threshold of 0.05 was applied. Subgroup analyses based on atopy and smoking status revealed statistical significance, suggesting that more comprehensive models may offer improved performance compared to univariate logistic models when accounting for these factors.

The Hosmer–Lemeshow goodness-of-fit test was applied to assess calibration in univariate models (Table 3). While slight miscalibration was noted in subgroups defined by allergy and smoking status, the models were well-calibrated overall.

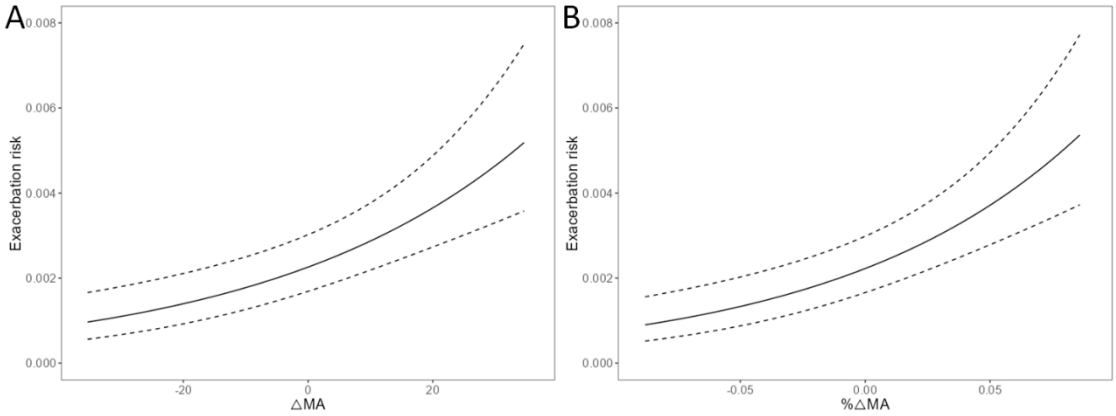

Figure 4. Prediction curves for ΔMA and %ΔMA

The vertical axis represents the risk of exacerbation occurring the following day, while the horizontal axis displays the independent variables ΔMA or %ΔMA. The dashed line indicates the 95% prediction interval for exacerbation risk.

Predicted risk curves based on ΔMA and %ΔMA (Figure 4) revealed a steady increase in exacerbation risk as the values of ΔMA and %ΔMA rose, confirming their reliability in predicting asthma exacerbation risk.

Discussion

In chapter 1 of this study, we analyzed PEF data from the Hi-CARAT cohort of patients with severe asthma to identify optimal predictors for asthma exacerbation. We evaluated the discriminative power of several previously proposed indicators, including the PEF slope, %predPEF, Min/Max, and CV. Additionally, we introduced two novel predictors, ΔMA and %ΔMA, which are simple to compute and demonstrated superior predictive performance compared to the existing indicators.

The key findings from this part of the study are as follows. First, both %ΔMA and ΔMA consistently outperformed other indicators in predicting real-time asthma exacerbations, as evidenced by higher AUC values, regardless of whether univariate or multivariate models were used. Furthermore, these predictors require minimal computational effort compared to the PEF slope, which relies on linear regression analysis. This simplicity makes %ΔMA and ΔMA strong candidates for future exacerbation prediction models. Second, when predicting real-time asthma exacerbations, the trend in PEF trajectories appeared to be a more reliable predictor than variability-focused indicators, such as CV. While variability-based predictors showed weaker discriminative performance, conflicting with earlier findings (Thamrin et al., 2010) , this discrepancy may stem from differences in study populations. Our study exclusively involved Asian patients with severe asthma residing in Hokkaido Prefecture, Japan. Third, relying solely on a single predictor from PEF data, whether it be %ΔMA, ΔMA, or the 14-day slope, is insufficient for optimal discriminative performance. This underscores the need for multivariate approaches to enhance prediction accuracy. Fourth, due to the complexity of asthma exacerbation onset, univariate models based on single predictors from PEF data fall short in accurately forecasting exacerbations. This limitation was evident in subgroup analyses, as the Hosmer–Lemeshow test revealed weak calibration in atopy-negative and never-smoker subgroups. Multivariate regression models further reinforced this finding, with the inclusion of covariates such as atopy and smoking status raising the AUC to 0.716. Both multivariate and mixed models demonstrated superior discriminative performance compared to univariate models. However, the complexity of these models necessitates computer use, which compromises simplicity. Moreover, establishing random effects in mixed models requires prior knowledge of a patient's exacerbation history.

Our earlier work has shown associations between asthma exacerbations and biomarkers like PBE and FeNO (Kimura et al., 2018; Kimura et al., 2021). However, these biomarkers are more suited for identifying clinical phenotypes rather than predicting the timing of exacerbations, as they lack time-dependent variables. In contrast, daily measurable indices such as PEF provide a practical means of predicting exacerbation

timing. Focusing PEF monitoring efforts on patients with clinical phenotypes prone to exacerbations may facilitate the development of prevention strategies.

There are, however, several limitations to this study. PEF data were recorded twice daily—once in the morning and once in the evening—with raw values used in the analysis. These measurements may be subject to operational errors, potentially affecting data quality. Accurate prediction of exacerbations relies on patients consistently and correctly recording their PEF values. However, adherence rates in real-world settings are often low, with studies reporting rates below 50% (Verschelden et al., 1996). Additionally, the computational demands of multivariate models limit their clinical applicability. The increasing adoption of smartphone-based portable PEF meters offers a potential solution to these issues (Natarajan et al., 2016). These devices can automate PEF data recording and validation, calculate exacerbation risks, and reduce the impact of operational errors and non-adherence. Future efforts should focus on developing predictive models tailored to such technologies to improve asthma management. Another limitation of the Hi-CARAT study is the lack of detailed data on the timing of fast-acting bronchodilator use. Exacerbations were defined based on systemic corticosteroid use for more than three days and/or hospitalization due to severe exacerbations, which restricted our ability to explore additional predictors, such as post-bronchodilator PEF response percentages. Furthermore, the absence of daily symptom diaries in the Hi-CARAT study prevented direct comparisons between our proposed model and symptom diary-based asthma control tools, such as the Asthma Symptom Utility Index. Developing a model that integrates both subjective and objective indicators remains a goal for future research.

Chapter 2 Patients' Categorization and Vulnerability Prediction Model

Introduction

The methodologies for assessing patients' vulnerability have advanced significantly in recent years, evolving to better address the complexities of survival data. The Cox proportional hazards model, introduced by Cox in 1972, has been a cornerstone of survival analysis (Cox, 1972). However, its applicability is limited when dealing with time-dependent covariates. To address this, Andersen and Gill extended the Cox model, proposing the Andersen-Gill model, which allows for the inclusion of time-dependent covariates and the analysis of recurrent event data (Andersen and Gill, 1982). This model is particularly suitable for exogenous time-dependent covariates. When time-dependent covariates are endogenous, meaning their values may be influenced by unobserved factors and correlated with survival time, the joint modeling framework becomes necessary. Joint models simultaneously account for longitudinal and survival data, effectively addressing issues associated with endogenous covariates (Wulfsohn and Tsiatis, 1997). Building on this, Lin et al. introduced the latent class joint model, an advancement of the traditional joint modeling framework (Lin et al., 2002). By incorporating latent classes, this approach captures heterogeneity among study subjects and provides a more precise tool for analyzing endogenous time-dependent covariates and time-to-event data. A limited number of studies have implemented PEF trajectories to assess individual vulnerability to exacerbation, despite advancements in methodology. It may because analyzing both endogenous time-dependent covariate (e.g., PEF) and time-to-event data using above mentioned methods is complex. For example, previous research has used covariates derived from PEF monitoring with the Anderson–Gill model to evaluate how these covariates associated to the hazard of exacerbation happened (Leander et al., 2021). Despite these advancements, extracting actionable information from PEF data, predicting exacerbations in real-time, and assessing patient vulnerability remain challenging for researchers and healthcare workers. To address the current research gap, we modified the LCJM for patients categorization based on their PEF trajectory and access their vulnerability to exacerbation in this part.

Materials and Methods

Statistical analyses

We constructed a LCJM to categorize patients and predict their vulnerability to exacerbations. The LCJM framework was developed to accommodate both time-dependent endogenous covariates and heterogeneity among study subjects (Lin et al., 2002). However, since changes in slopes—specifically, decreasing trends—were observed in the PEF trajectories of some participants, the linear longitudinal submodel proposed by Lin et al. was not able to provide an adequate fit. To address this issue, we modified the LCJM to better analyze the PEF trajectories and evaluated its performance in simulation study.

The observed dataset in our simulation setting

The participant index is denoted by *i*, ranges from 1 to n. We use *j* to represent the index of the tracing period for participant *i*, where *j* ranges from 1 to n_i. In our simulation setting, the total number of participants was set to 100, with each participant being traced 5 times, resulting in 500 time-to-event observations. The dataset observed for participant *i* during their *j*-th tracing period is represented as:

$$\{\boldsymbol{y_{ij}}, T_{ij}, \delta_{ij}, \boldsymbol{v_i}, \boldsymbol{Z_i}, \boldsymbol{W_{ij}}(k)\}.$$

$\boldsymbol{y_{ij}} = [y_{ij1} \quad \cdots \quad y_{ijk} \quad \cdots \quad y_{ijn_{ij}}]^{\mathrm{T}}$ denotes the time-dependent PEF monitoring data. The unit of time was denoted by *k*. The range of k was setting as [0.1, 30] and the unit of k is 0.1. Thus, a maximum of 300 longitudinal observations were collected for each participant. The total number of PEF observations collected from participant *i* during their *j*-th tracing period is n_{ij}.

T_{ij} represents the time-to-event data, recording the time when an exacerbation or censoring occurred. Setting the beginning of a tracing period *j* as $k = 1$, T_{ij} ranges from 1 to n_{ij}. The variable δ_{ij} serves as the censoring indicator, where $\delta_{ij} = 1$ indicates the occurrence of an event, while $\delta_{ij} = 0$ denotes censoring. $\boldsymbol{v_i}$ and $\boldsymbol{Z_i}$ are design matrices that contain the independent variables, while the time-dependent covariates are denoted by $\boldsymbol{W_{ij}}(k)$.

Model specification

We specified the logistic submodel in the LCJM as follows:

$$c_i \sim Bernoulli(\pi_i)$$

$$\pi_i = P(c_i = 1) = \frac{exp(\boldsymbol{v_i^T \eta})}{1 + exp(\boldsymbol{v_i^T \eta})}, \qquad P(c_i = 0) = \frac{1}{1 + exp(\boldsymbol{v_i^T \eta})}.$$

Here, c_i denotes the unobserved category from which participant *i* is recruited, and c_i follows a Bernoulli distribution. The parameter $\boldsymbol{\eta}$ is a vector of regression coefficients with a dimension of $q_{\boldsymbol{\eta}}$. We assume that asthma patients exhibit two distinct patterns in

their PEF trajectories. Participants in unresponsive group $(c_i = 0)$ whose PEF trajectories are unresponsive to upcoming exacerbation show a flat line of PEF observations with measurement error, while participants in responsive group $(c_i = 1)$ may display segmented lines of PEF values recorded during one or more tracing periods. Based on this assumption, the longitudinal submodel in the LCJM is specified as a segmented linear model:

$$y_{ij}(k) = \beta_{0i} + c_i\beta_{1i}\big(k - \tau_{ij}\big)I\big(k > \tau_{ij}\big) + \varepsilon_{ij}(k)$$

Here, τ_{ij} represents the change point in the slope, and *I* is the indicator function. Given that the variance of PEF measurements varies between individuals, we assume that $\varepsilon_{ij}(k) \sim N(0, \sigma_{ei}^2)$. The longitudinal observations were generated using the segmented linear model.

However, the parameter β_{1i} is highly dependent on the parameter τ_{ij} and cannot be estimated when $\tau_{ij} > \max(k)$, which results in convergence issues during parameter estimation. Therefore, in addition to the segmented model, we opted for an additive model to fit the PEF trajectories:

$$y_{ij}(k) = \sum_{m=1}^{h_{ij}} b_m(k)\beta_{ijm} + \varepsilon_{ij}(k)$$

$$\varepsilon_{ij}(k) \sim N(0, \sigma_{ei}^2).$$

Here, the knots are denoted by $\{x_{ijm} : m = 1, \ldots, h_{ij}\}$, where *m* is the index of the knots, and h_{ij} is the total number of knots for participant *i* in their *j*-th tracing period. We set the knots such that there are four PEF observations per interval. The function $b_m(k)$ represents the tent basis function defined as:

$$b_m(k) = \begin{cases} (k - x_{ij(m-1)})/(x_{ijm} - x_{ij(m-1)}), & x_{ij(m-1)} < k \le x_{ijm} \\ (x_{ij(m+1)} - k)/(x_{ij(m+1)} - x_{ijm}), & x_{ijm} < k \le x_{ij(m+1)} \\ 0, & otherwise \end{cases}$$

while

$$b_1(k) = \begin{cases} (x_{ij2} - k)/(x_{ij2} - x_{ij1}), & k < x_{ij2} \\ 0, & otherwise \end{cases}$$

and

$$b_{h_{ij}}(k) = \begin{cases} (k - x_{ij(h_{ij}-1)})/(x_{ijh_{ij}} - x_{ij(h_{ij}-1)}), & k > x_{ij(h_{ij}-1)} \\ 0, & otherwise. \end{cases}$$

The parameters $\boldsymbol{\beta}$ were estimated using the maximum likelihood approach.

Similar to the conventional joint model, an association term (ASC) is shared between the longitudinal submodel and the time-to-event submodel (Wulfsohn and Tsiatis, 1997). We

defined the association term as the relative difference between the participant's personal PEF median and the predicted value $y_{ij}(k)$ from the longitudinal model:

$$ASC_{ij}(k) = \frac{\left(\sum_{m=1}^{h_{ij}} b_m(k)\beta_{ijm} - PEFMedian_i\right)}{PEFMedian_i}.$$

Assuming that participants in category 0 and category 1 have different baseline hazards and covariates, the hazard function for the heterogeneous study population is defined as follows:

$$\begin{cases} h_0(k)exp\left(\boldsymbol{Z_i\gamma_0} + \boldsymbol{\gamma_{l0}M_{ij}}(k)\right), & when\ c_i = 0, \\ h_1(k)exp\left(\boldsymbol{Z_i\gamma_1} + \boldsymbol{\gamma_{l1}M_{ij}}(k)\right), & when\ c_i = 1. \end{cases}$$

Here, $h_0(k)$ and $h_1(k)$ are the baseline hazard functions for participants in category 0 and category 1, respectively. $\boldsymbol{Z_i}$ represents the time-independent covariates, while $\boldsymbol{M_{ij}}(k)$ denotes the collection of time-dependent variables. The parameter $\boldsymbol{\gamma}$ are the regression coefficients. For participants in unresponsive group $(c_i = 0)$, we included pseudo baseline age and time-dependent temperature data as covariates. For participants in responsive group $(c_i = 1)$, the covariates included pseudo data whether a positive outcome was observed in the ATOPY test, as well as the association term (ASC).

We assumed that the baseline hazard function in the time-to-event submodel follows a Weibull distribution, defined as:

$$h_{c_i}(t) = \lambda_{c_i}^2 \rho_{c_i} u^{\rho_{c_i}-1}$$

indicating that participants from different categories may have different baseline hazard functions. We used $\lambda_{c_i}^2$ instead of λ_{c_i} to improve convergence performance.

We adjusted the covariates and parameter scales to ensure that all events occurred before k=30 in our simulations. The simulation parameter settings are summarized in Table 4.

Table 4. Simulation Parameter Settings

Parameter	Setting
Parameters in the logistic submodel	
η_1	$\eta_1 = 1$
η_2	$\eta_2 = 1$
Parameters in the longitudinal submodel	
β_{0i}	$\beta_{0i} \sim Uniform(1,5)$
β_{1i}	$\beta_{1i} \sim Uniform(-1,-0.5)$
τ_{ij}	$\tau_{ij} \sim Uniform(-0.5,18)$
σ_{ei}	$\sigma_{ei} \sim Uniform(0.1,0.3)$

Parameters in the survival submodel	
λ_0	$\lambda_0 = 0.2$
ρ_0	$\rho_0 = 1$
γ_{01}	$\gamma_{01} = 1$
γ_{02}	$\gamma_{02} = 1$
λ_1	$\lambda_1 = 0.1$
ρ_1	$\rho_1 = 1.1$
γ_{11}	$\gamma_{11} = 1$
γ_{12}	$\gamma_{12} = 1$

This table outlines how the parameters in our model were set or generated.

With the model specification finalized, we will next outline the strategy employed for estimating the parameters. Let $\boldsymbol{\Theta}$ denote the combination of parameters and $\breve{\boldsymbol{X}}$ denote the combination of observed independent variables respectively:

$$\boldsymbol{\Theta} = \{\boldsymbol{\eta}, \boldsymbol{\beta}, \boldsymbol{\Sigma_e}, \boldsymbol{\gamma_0}, \boldsymbol{\gamma_1}, \boldsymbol{\gamma_{l0}}, \boldsymbol{\gamma_{l1}}\}, \qquad \breve{\boldsymbol{X}} = \{\boldsymbol{v}, \boldsymbol{Z}, \boldsymbol{W}\}.$$

The complete-data likelihood function can then be expressed as:

$$f(\boldsymbol{Y}, \boldsymbol{T}, \boldsymbol{\delta}, \boldsymbol{c}|\boldsymbol{\Theta}; \breve{\boldsymbol{X}}) = f(\boldsymbol{c}|\boldsymbol{\Theta}; \breve{\boldsymbol{X}})\, f(\boldsymbol{Y}, \boldsymbol{T}, \boldsymbol{\delta}|\boldsymbol{\Theta}; \breve{\boldsymbol{X}}, \boldsymbol{c}).$$

Assuming conditional independence, we have:

$$f(\boldsymbol{Y}, \boldsymbol{T}, \boldsymbol{\delta}|\boldsymbol{\Theta}; \breve{\boldsymbol{X}}, \boldsymbol{c}) = f(\boldsymbol{Y}|\boldsymbol{\Theta}; \breve{\boldsymbol{X}}, \boldsymbol{c}) f(\boldsymbol{T}, \boldsymbol{\delta}|\boldsymbol{\Theta}; \breve{\boldsymbol{X}}, \boldsymbol{c})$$

Thus, the complete-data likelihood function simplifies to:

$$f(\boldsymbol{Y}, \boldsymbol{T}, \boldsymbol{\delta}, \boldsymbol{c}|\boldsymbol{\Theta}; \breve{\boldsymbol{X}}) = f(\boldsymbol{c}|\boldsymbol{\Theta}; \breve{\boldsymbol{X}})\, f(\boldsymbol{Y}|\boldsymbol{\Theta}; \breve{\boldsymbol{X}}, \boldsymbol{c}) f(\boldsymbol{T}, \boldsymbol{\delta}|\boldsymbol{\Theta}; \breve{\boldsymbol{X}}, \boldsymbol{c})$$

We further assume that observations from each participant are independent, and that observations from different tracing periods of the same participant are independent given $\boldsymbol{\Theta}$, $\breve{\boldsymbol{X}}$, and $\boldsymbol{c}$. Thus, the complete-data likelihood function can be derived as:

$$f(\boldsymbol{Y}, \boldsymbol{T}, \boldsymbol{\delta}, \boldsymbol{c}|\boldsymbol{\Theta}; \breve{\boldsymbol{X}}) = \prod_{i=1}^{n} f(c_i|\boldsymbol{\Theta_i}; \breve{\boldsymbol{X}}_{\boldsymbol{i}}) \prod_{j=1}^{n_i} f(T_{ij}, \delta_{ij}|\boldsymbol{\Theta_{ij}}; \breve{\boldsymbol{X}}_{\boldsymbol{ij}}, c_i) \prod_{k=0}^{n_{ij}} f(y_{ijk}|\boldsymbol{\Theta_{ij}}; \breve{\boldsymbol{X}}_{\boldsymbol{ij}}, c_i)$$

The corresponding log-likelihood function is given by:

$$logf(\boldsymbol{Y}, \boldsymbol{T}, \boldsymbol{\delta}, \boldsymbol{c}|\boldsymbol{\Theta}; \breve{\boldsymbol{X}})$$

$$= \sum_{i=1}^{n} logf(c_i|\boldsymbol{\Theta_i}; \breve{\boldsymbol{X}}_{\boldsymbol{i}}) + \sum_{i=1}^{n} \sum_{j=1}^{n_i} logf(T_{ij}, \delta_{ij}|\boldsymbol{\Theta_{ij}}; \breve{\boldsymbol{X}}_{\boldsymbol{ij}}, c_i)$$

$$+ \sum_{i=1}^{n} \sum_{j=1}^{n_i} \sum_{k=0}^{n_{ij}} logf(y_{ijk}|\boldsymbol{\Theta_{ij}}; \breve{\boldsymbol{X}}_{\boldsymbol{ij}}, c_i).$$

By expanding each term, we derived the analytical forms for the logistic submodel and

the longitudinal submodel. For the logistic submodel:

$$log\{f(\boldsymbol{c}|\boldsymbol{\eta};\boldsymbol{v})\} = \sum_{i=1}^{n}\left[c_i\boldsymbol{v_i^T}\boldsymbol{\eta} - log\{1 + exp(\boldsymbol{v_i^T}\boldsymbol{\eta})\}\right].$$

For the longitudinal submodel:

$$log\{f(\boldsymbol{Y}|\boldsymbol{\Sigma_e},\boldsymbol{\beta};\boldsymbol{c})\}$$

$$= -\frac{1}{2}\sum_{i=1}^{n}\sum_{j=1}^{n_i}\{n_{ij}log(2\pi) + log(\sigma_{ei}^2)\} + \sum_{i=1}^{n}\sum_{j=1}^{n_i}\sum_{k=0}^{n_{ij}}\frac{\left\{y_{ij}(k) - \sum_{m=1}^{h_{ij}} b_m(k)\beta_m\right\}^2}{-2\sigma_{ei}^2}.$$

For the time-to-event submodel, the survival function is defined as:

$$S_{c_i}\left(k|\boldsymbol{Z_i},\boldsymbol{M_{ij}}(k)\right) = exp\left(-\int_0^k h_{c_i}(u)exp\left(\boldsymbol{Z_i}\boldsymbol{\gamma}_{c_i} + \boldsymbol{\gamma}_{lc_i}\boldsymbol{M_{ij}}(u)\right)du\right).$$

Thus, the log-likelihood function for the time-to-event submodel is given by:

$$log\{f(\boldsymbol{T},\boldsymbol{\delta}|\boldsymbol{\Theta};\boldsymbol{Z_i},\boldsymbol{M_{ij}}(k),c_i)\}$$

$$= \sum_{i=1}^{n}\sum_{j=1}^{n_i}\left[\delta_{ij}\left\{log\left(h_{c_i}(T_{ij})\right) + \boldsymbol{Z_i}\boldsymbol{\gamma}_{c_i} + \boldsymbol{\gamma}_{lc_i}\boldsymbol{M_{ij}}(T_{ij})\right\}\right.$$

$$\left. - \int_0^{T_{ij}} h_{c_i}(u)exp\left(\boldsymbol{Z_i}\boldsymbol{\gamma}_{c_i} + \boldsymbol{\gamma}_{lc_i}\boldsymbol{M_{ij}}(u)\right)du\right]$$

We adopted a two-step parameter estimation approach. First, we estimated $\boldsymbol{\beta}$ and $\boldsymbol{\Sigma_e}$ by maximizing the likelihood function of the longitudinal submodel, obtaining their estimates $\widehat{\boldsymbol{\beta}}$ and $\widehat{\boldsymbol{\Sigma}}_{\boldsymbol{e}}$. After that, the association term shared between the longitudinal submodel and the time-to-event submodel was predicted as follows:

$$ASC\_pred_{ij}(k) = \frac{\left(\sum_{m=1}^{h_{ij}} b_m(k)\hat{\beta}_{ijm} - YMedian_i\right)}{YMedian_i}$$

By incorporating the association term prediction into the time-to-event submodel, we then simultaneously estimate the parameters of both the logistic submodel and the survival submodel.

Expectation–maximization algorithm

However, the likelihood functions of the logistic submodel and time-to-event submodel cannot be directly maximized because the latent category $\boldsymbol{c}$ is unobserved. To address this issue, we implemented the Expectation-Maximization (EM) algorithm (Dempster et al., 1977). Assuming that observations from each individual are independent, the marginal log-likelihood function can be obtained by integrating the joint likelihood function over $\boldsymbol{c}$:

$$\log\{f(\boldsymbol{T},\boldsymbol{\delta}|\boldsymbol{\Theta};\breve{\boldsymbol{X}})\} = \sum_{i=1}^{n}\log\left\{\sum_{c_i} f(\boldsymbol{T_i},\boldsymbol{\delta_i},c_i|\boldsymbol{\Theta};\breve{\boldsymbol{X}})\right\}$$

Applying the conditional expectation, we can express it as:

$$\log\{f(\boldsymbol{T},\boldsymbol{\delta}|\boldsymbol{\Theta};\breve{\boldsymbol{X}})\} = \sum_{i=1}^{n}\log\left[E_{c_i|\boldsymbol{\Theta};\breve{\boldsymbol{X}},\boldsymbol{T_i},\boldsymbol{\delta_i}}\left\{\frac{f(\boldsymbol{T_i},\boldsymbol{\delta_i},c_i|\boldsymbol{\Theta};\breve{\boldsymbol{X}})}{f(c_i|\boldsymbol{\Theta};\breve{\boldsymbol{X}},\boldsymbol{T_i},\boldsymbol{\delta_i})}\right\}\right]$$

where E denotes the expectation function. To simplify the computation, we apply Jensen's Inequality (Jensen, 1906) to obtain a lower bound, which we then maximize:

$$log\left[E_{c_i|\boldsymbol{\Theta};\breve{\boldsymbol{X}},\boldsymbol{T_i},\boldsymbol{\delta_i}}\left\{\frac{f(\boldsymbol{T_i},\boldsymbol{\delta_i},c_i|\boldsymbol{\Theta};\breve{\boldsymbol{X}})}{f(c_i|\boldsymbol{\Theta};\breve{\boldsymbol{X}},\boldsymbol{T_i},\boldsymbol{\delta_i})}\right\}\right] \geq E_{c_i|\boldsymbol{\Theta};\breve{\boldsymbol{X}},\boldsymbol{T_i},\boldsymbol{\delta_i}}\left[log\left\{\frac{f(\boldsymbol{T_i},\boldsymbol{\delta_i},c_i|\boldsymbol{\Theta};\breve{\boldsymbol{X}})}{f(c_i|\boldsymbol{\Theta};\breve{\boldsymbol{X}},\boldsymbol{T_i},\boldsymbol{\delta_i})}\right\}\right]$$

Thus, the objective function for the E-step of the EM algorithm is:

$$\sum_{i=1}^{n}\left[E_{c_i|\boldsymbol{\Theta}^{(s)};\breve{\boldsymbol{X}},\boldsymbol{T_i},\boldsymbol{\delta_i}}\left[log\{f(\boldsymbol{T_i},\boldsymbol{\delta_i},c_i|\boldsymbol{\Theta};\breve{\boldsymbol{X}})\}\right] - E_{c_i|\boldsymbol{\Theta}^{(s)};\breve{\boldsymbol{X}},\boldsymbol{T_i},\boldsymbol{\delta_i}}\left[log\{f(c_i|\boldsymbol{\Theta};\breve{\boldsymbol{X}},\boldsymbol{T_i},\boldsymbol{\delta_i})\}\right]\right]$$

Since $E_{c_i|\boldsymbol{\Theta}^{(s)};\breve{\boldsymbol{X}},\boldsymbol{T_i},\boldsymbol{\delta_i}}\left[log\{f(c_i|\boldsymbol{\Theta};\breve{\boldsymbol{X}},\boldsymbol{T_i},\boldsymbol{\delta_i})\}\right]$ is fixed given $\boldsymbol{\Theta_i} = \boldsymbol{\Theta_i^{(s)}}$, the function simplifies to:

$$Q(\boldsymbol{\Theta}|\boldsymbol{\Theta}^{(s)}) = \sum_{i=1}^{n}\left[E_{c_i|\boldsymbol{\Theta}_i^{(s)};\breve{\boldsymbol{X}},\boldsymbol{T_i},\boldsymbol{\delta_i}}\left[log\{f(\boldsymbol{T_i},\boldsymbol{\delta_i},c_i|\boldsymbol{\Theta};\breve{\boldsymbol{X}})\}\right]\right]$$

This can be expressed as:

$$= \sum_{i=1}^{n}\sum_{c_i} f\left(c_i|\boldsymbol{\Theta}_i^{(s)};\breve{\boldsymbol{X}},\boldsymbol{T_i},\boldsymbol{\delta_i}\right) log f(\boldsymbol{T_i},\boldsymbol{\delta_i},c_i|\boldsymbol{\Theta};\breve{\boldsymbol{X}})$$

where the posterior distribution of c_i given $\boldsymbol{\Theta}_i^{(s)},\breve{\boldsymbol{X}},\boldsymbol{T_i},\boldsymbol{\delta_i}$, can be computed using Bayes' Theorem:

$$f\left(c_i|\boldsymbol{\Theta}_i^{(s)};\breve{\boldsymbol{X}},\boldsymbol{T_i},\boldsymbol{\delta_i}\right) = \frac{f\left(c_i\middle|\boldsymbol{\Theta}_i^{(s)};\breve{\boldsymbol{X}}\right) f\left(\boldsymbol{T_i},\boldsymbol{\delta_i}\middle|\boldsymbol{\Theta}_i^{(s)};\breve{\boldsymbol{X}},c_i\right)}{\sum_{c_i=0}^{1} f\left(c_i\middle|\boldsymbol{\Theta}_i^{(s)};\breve{\boldsymbol{X}}\right) f\left(\boldsymbol{T_i},\boldsymbol{\delta_i}\middle|\boldsymbol{\Theta}_i^{(s)};\breve{\boldsymbol{X}},c_i\right)}$$

We used the gradient-based optimization method, Limited-memory Broyden–Fletcher–Goldfarb–Shanno with Box constraints (L-BFGS-B), to maximize the function Q and estimate the model parameters (Liu and Nocedal, 1989). The gradients of each parameter were calculated to accelerate convergence:

Gradient with respect to $\eta_{q_{\boldsymbol{\eta}}}$:

$$\frac{\partial \boldsymbol{Q}(\boldsymbol{\Theta}|\boldsymbol{\Theta}^{(s)})}{\partial \eta_{q_{\boldsymbol{\eta}}}} = \sum_{i=1}^{n}\left[\sum_{c_i} f\left(c_i|\boldsymbol{\Theta}_i^{(s)}; \breve{\boldsymbol{X}}, \boldsymbol{T_i}, \boldsymbol{\delta_i}\right)\left\{c_i v_{iq_\eta} - \frac{v_{iq_{\boldsymbol{\eta}}}}{1+exp(-\boldsymbol{v_i^T \eta})}\right\}\right].$$

Gradient with respect to λ_{c_i}:

$$\frac{\partial \boldsymbol{Q}(\boldsymbol{\Theta}|\boldsymbol{\Theta}^{(s)})}{\partial \lambda_{c_i}} = \sum_{i=1}^{n} f\left(c_i|\boldsymbol{\Theta}_i^{(s)}; \breve{\boldsymbol{X}}, \boldsymbol{T_i}, \boldsymbol{\delta_i}\right) \times$$

$$\sum_{j=1}^{n_i}\left[\frac{2\delta_{ij}}{\lambda_{c_i}} - \int_0^{T_{ij}} 2\lambda_{c_i}\rho_{c_i}u^{\rho_{c_i}-1} exp\left(\boldsymbol{Z_i\gamma}_{c_i} + \boldsymbol{\gamma}_{\boldsymbol{lc_i}}\boldsymbol{M_{ij}}(u)\right)du\right].$$

Gradient with respect to ρ_{c_i}:

$$\frac{\partial \boldsymbol{Q}(\boldsymbol{\Theta}|\boldsymbol{\Theta}^{(s)})}{\partial \rho_{c_i}} = \sum_{i=1}^{n} f\left(c_i|\boldsymbol{\Theta}_i^{(s)}; \breve{\boldsymbol{X}}, \boldsymbol{T_i}, \boldsymbol{\delta_i}\right) \times$$

$$\sum_{j=1}^{n_i}\left[\frac{\delta_{ij}}{\rho_{c_i}} + \delta_{ij}log(T_{ij})\right.$$

$$\left. - \int_0^{T_{ij}} \lambda_{c_i}^2\left\{u^{\rho_{c_i}-1}\rho_{c_i}log(u) + u^{\rho_{c_i}-1}\right\} exp\left(\boldsymbol{Z_i\gamma}_{c_i} + \boldsymbol{\gamma}_{\boldsymbol{lc_i}}\boldsymbol{M_{ij}}(u)\right)du\right].$$

Gradient with respect to γ_{ciq_γ}:

$$\frac{\partial \boldsymbol{Q}(\boldsymbol{\Theta}|\boldsymbol{\Theta}^{(s)})}{\partial \gamma_{ciq_\gamma}} = \sum_{i=1}^{n} f\left(c_i|\boldsymbol{\Theta}_i^{(s)}; \breve{\boldsymbol{X}}, \boldsymbol{T_i}, \boldsymbol{\delta_i}\right) \times$$

$$\sum_{j=1}^{n_i}\left[Z_{q_\gamma}\delta_{ij} - \int_0^{T_{ij}} \lambda_{c_i}^2\rho_{c_i}u^{\rho_{c_i}-1}Z_{q_\gamma} exp\left(\boldsymbol{Z_i\gamma_{c_i}} + \boldsymbol{\gamma_{lc_i}}\boldsymbol{M_{ij}}(u)\right)du\right].$$

In the M-step, parameters are updated according to:

$$\boldsymbol{\Theta}^{(\boldsymbol{s+1})} = \underset{\Theta}{\text{argmax}} Q\left(\boldsymbol{\Theta}|\boldsymbol{\Theta}^{(s)}\right).$$

as the EM algorithm iterates, the parameter estimates gradually converge to the maximum likelihood estimates.

C-index and model evaluation

Using the estimates of η, we first predicted $\hat{\pi}_i$, the probability that $c_i = 1$

$$\hat{\pi}_i = P(c_i = 1) = \frac{exp\left(\boldsymbol{v_i^T}\,\hat{\boldsymbol{\eta}}\right)}{1 + exp(\boldsymbol{v_i^T}\,\hat{\boldsymbol{\eta}})}$$

A higher $\hat{\pi}_i$ indicates that individual *i* is more likely to belong to latent category 1. Based

on the predicted $\hat{\pi}_i$ values, participants can be ranked from the highest to lowest probability of being in category 1. We then evaluated all possible cut-off values for $\hat{\pi}_i$ and calculated the corresponding C-index for dividing participants into categories 0 and 1, respectively. The C-index for each category (c_i) is defined as:

$$C_{c_i} = \frac{\sum_{ij}\sum_{i'j'}\delta_{ij}I(T_{ij} < T_{i'j'})I\left(\int_0^{T_{ij}} \boldsymbol{Z_i\gamma_{c_i}} + \boldsymbol{\gamma_{lc_i}M_{ij}}(u)du > \int_0^{T_{ij}} \boldsymbol{Z_{i'}\gamma_{c_{i'}}} + \boldsymbol{\gamma_{lc_{i'}}M_{i'j'}}(u)du\right)}{\sum_{ij}\sum_{i'j'}\delta_{ij}I(T_{ij} < T_{i'j'})}.$$

This C-index is a modified version of the Gönen and Heller C-index (Gönen and Heller, 2005). We also defined an overall indicator, the integrated C-index, as follows:

$$C_{integ} = \frac{C_0 \times Num\ T\ in\ the\ category\ 0 + C_1 \times Num\ T\ in\ the\ category\ 1}{The\ total\ \ Num\ T}.$$

In the equation above, $Num\ T$ represents the number of time-to-event observations. The cut-off value for π that maximizes C_{integ} was chosen for categorizing participants.

We simulated two censoring scenarios: no censoring and right censoring at k=10. The no-censoring scenario simulates the condition where asthma patients continuously perform long-term PEF monitoring, while the right-censoring scenario simulates a typical cohort study setting. Both scenarios were iterated 1000 times, and the performance of parameter estimation was evaluated. Since the true latent categories of participants were known in our simulation setting, we also assessed the model's performance in discriminating latent categories by calculating the c-index. Additionally, Kaplan-Meier curves were plotted based on both the true categories and the predicted categories (Kaplan and Meier, 1958). All statistical analyses in this section were conducted using R version 4.3.2 (R Development Core Team, 2019).

Results

The Table 5 presents the parameter estimation results from the simulation study.

Table 5. Parameter estimation in simulation study

Par	No censoring scenario					Right censoring scenario			
	True value	Bias	ASE	ESE	CP	Bias	ASE	ESE	CP
η_1	1.000	0.082	0.438	0.358	0.916	0.201	0.674	0.395	0.995
η_2	1.000	0.092	0.433	0.329		0.136	0.624	0.356	
λ_0	0.200	-0.023	0.033	0.033		-0.038	0.035	0.030	
λ_1	0.100	0.045	0.020	0.016		0.043	0.025	0.020	
ρ_0	1.000	0.191	0.145	0.148		0.256	0.155	0.157	
ρ_1	1.100	-0.112	0.084	0.066		-0.115	0.110	0.091	
γ_{01}	1.000	-0.043	0.223	0.217		0.062	0.335	0.232	
γ_{02}	1.000	-0.152	0.084	0.085		-0.192	0.097	0.096	
γ_{11}	1.000	-0.184	0.171	0.135		-0.206	0.254	0.183	
γ_{12}	1.000	-0.110	0.038	0.024		-0.087	0.048	0.030	

Average sample standard error (ASE) and coverage probability (CP) are based on 1000 iterations. Empirical standard error (ESE) is the average of parameter standard error estimates.

The proposed model demonstrated strong performance in parameter estimation, confirming its reliability. The stability of both average sample standard error (ASE) and empirical standard error (ESE) values indicates that the model consistently produces accurate parameter estimates across simulations. Furthermore, the consistency between ASE and ESE suggests that the model appropriately captures the uncertainty in parameter estimation. This result indicates that the model's performance remains robust even under different censoring scenarios.

Additionally, we evaluated the modified Gönen and Heller C-index for assessing the model's effectiveness in identifying asthma exacerbation vulnerability. The results are summarized in the Table 6.

Table 6. The Gönen and Heller c-index in simulation study

	No censoring scenario		Right censoring scenario	
	Mean	Standard error	Mean	Standard error
LCJM c-index (unresponsive group $(c_i = 0)$)	0.611	0.032	0.620	0.035
LCJM c-index	0.663	0.027	0.674	0.030

(responsive group $(c_i = 1)$)				
LCJM integrated c-index	0.646	0.021	0.655	0.023
Time-to-event model c-index (unresponsive group only)	0.544	0.022	0.550	0.024
Joint model c-index (responsive group only)	0.654	0.026	0.652	0.025

LCJM refers to the modified latent class joint model we proposed. The LCJM c-index (unresponsive group $(c_i = 0)$) denotes the Gönen and Heller c-index for participants classified as unresponsive group $(c_i = 0)$, while the LCJM c-index (responsive group $(c_i = 1)$) denotes the c-index for those classified as responsive group $(c_i = 1)$.

The LCJM integrated c-index is calculated by averaging the LCJM c-index for unresponsive group and responsive group, weighted by the corresponding number of time-to-event observations. The time-to-event model c-index (unresponsive group only) was calculated under the assumption that all participants belong to unresponsive group, whereas the joint model c-index (responsive group only) was calculated assuming all participants belong to responsive group.

The modified LCJM model demonstrated superior discriminant performance in identifying patients' vulnerability to event compared to conventional time-to-event and joint models. For participants classified into unresponsive group $(c_i = 0)$, the Gönen and Heller c-index was 0.611, while for those in responsive group $(c_i = 1)$, it was 0.663 under the no censoring scenario. When switch to the right censoring scenario, the c-index became 0.620 and 0.674 for unresponsive and unresponsive group respectively. The LCJM integrated c-index was 0.646 under the no censoring scenario and 0.655 under the right censoring scenario. In contrast, the conventional joint model, which assumes all participants belong to responsive group, yielded a c-index of 0.654. The time-to-event model, assuming all participants belong to unresponsive group and ignoring longitudinal covariates, showed an even lower c-index of 0.544.

We also evaluated the model's accuracy in category discrimination. In the no censoring scenario, the mean c-index for category discrimination was 0.956 with a standard error (SE) of 0.018. Under the right censoring scenario, the mean c-index slightly decreased to 0.955 with an SE of 0.019. These results indicate that our model provides accurate and robust predictions for categorizing participants, even in the presence of censored data.

Using simulation data generated in the first iteration, Kaplan-Meier survival curves were drawn based on both the true category and the predicted category.

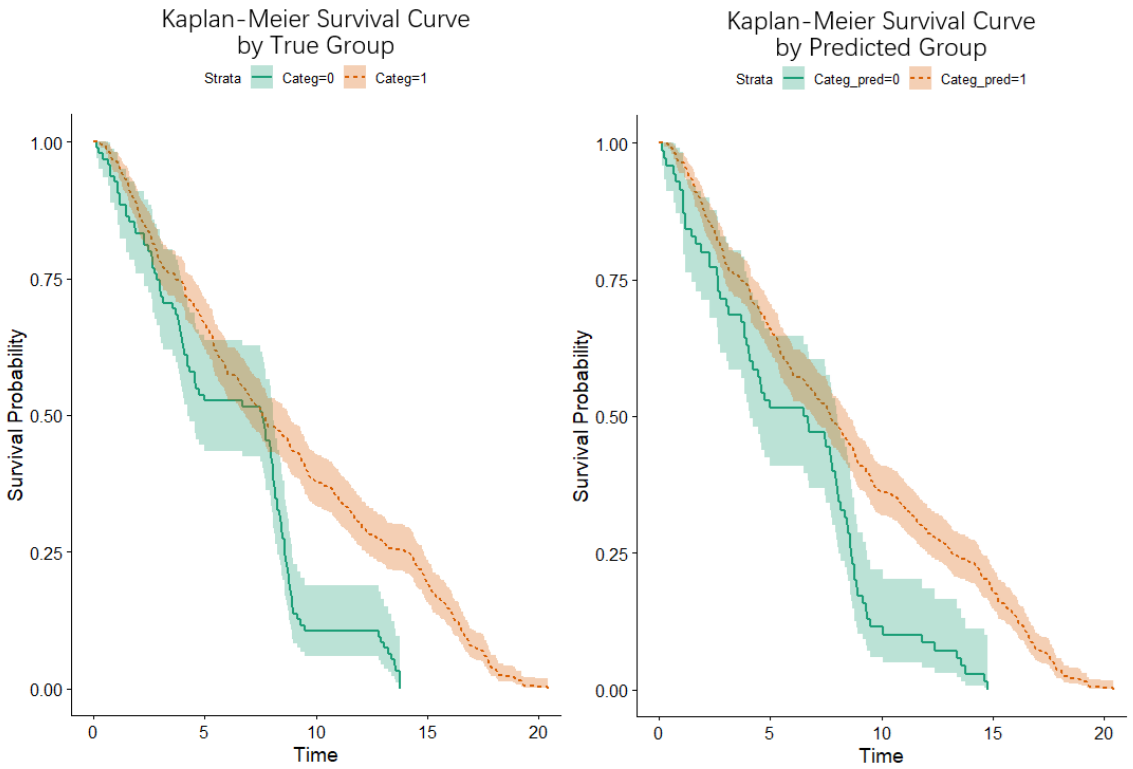

Figure 5. Kaplan-Meier survival curve using data from the first simulation

The left panel shows the strata Kaplan-Meier survival curve stratified by the true category of participants, while the right panel shows curves stratified by the predicted category. The shaded regions indicate the confidence intervals.

In both panels, the green solid line represents the survival curve for participants in unresponsive group, and the red dashed line represents those in responsive group. The similarity between the patterns in the left and right panels suggests that the model accurately predicts category membership when correctly specified. The overlap in the survival curves indicates that the predicted categories closely match the true categories.

Discussion

We developed a modified LCJM and evaluated its performance in terms of parameter estimation and discriminant ability. This model was used to assess individual vulnerability to asthma exacerbation while accounting for participant heterogeneity. Participants were classified into two groups, unresponsive group and responsive group, based on whether their PEF trajectories were responsive to impending exacerbations. In the simulation study, our model demonstrated high accuracy in parameter estimation, and participants categorization with c-index values of 0.956 and 0.955 in the non-censoring and right-censoring scenarios, respectively. Our model also achieving the best performance based on the Gönen and Heller c-index.

Our study has several limitations. Firstly, although we accounted for population heterogeneity, the classification of participants may still be overly simplified. There may be additional latent categories within the study population, suggesting that extending our logistic submodel to a multinomial logistic framework is a direction for future research. Secondly, the current model specification has limitations. Since the pathology of asthma exacerbation is still debated, we must select predictors from numerous candidates when construct the LCJM. To avoid the model mis-specification, developing a covariate selection strategy, such as using the least absolute shrinkage and selection operator for the LCJM, is an important area for future exploration (Tibshirani, 1996). Additionally, our model did not account for individual frailty in the survival analysis. We assumed that time-to-event data from different tracing periods of the same participant were mutually independent, which contradicts evidence suggesting that patients with a history of asthma exacerbations are more likely to experience future exacerbations (Engelkes et al., 2020). Finally, rather than applying the model into real-world datasets such as the Hi-CARAT datasets, we evaluated our model based on simulation study only.

Despite these limitations, we believe that our findings provide valuable insights for researchers and healthcare professionals interested in severe asthma PEF monitoring. We hope that our work will contribute to future analyses of PEF trajectories and help improve the management of asthma exacerbations.

Conclusion

The following findings were obtained from this study.

1) PEF monitoring data can be effectively used to perform the real-time exacerbation prediction in patients with severe asthma.
2) Novel predictive factors, ΔMA and %ΔMA, yielded the best predictive capabilities comparing to conventional statistics calculated from PEF trajectory.
3) By extending the LCJM framework to incorporate the heterogenous PEF trajectories, the vulnerability of patients with severe asthma to exacerbations can be assessed.
4) The modified LCJM framework demonstrated superior discriminative performance compared to the conventional joint model framework in simulation study.

We aim to further extend the LCJM by incorporating a multinomial logistic submodel and individual frailty effects, and applying the modified LCJM to real-world datasets such as the Hi-CARAT datasets in the next phase of our study. We hope the results of this study help in the construction of a clinically applicable exacerbation prediction model in the future.

Acknowledgement

I would like to express my deepest gratitude to my supervisor, Dr. Isao Yokota. I joined his lab in 2020. During the seminar held in the lab, I studied alongside early laboratory members Yoko Unoki, Kazufumi Okada and Tasuku Inao. Through these seminars, I acquired knowledge of generalized linear models, mixed models, and clinical prediction models, which significantly enhanced my statistical skills. The invaluable insights of Dr. Yokota into the epidemiology research area and his guidance on biostatistical methodology has always been of great help, particularly when challenges arose during my research. His unwavering support and encouragement have been crucial throughout this research.

I am also sincerely thankful to my co-authors, Prof. Satoshi Konno, Dr. Hirokazu Kimura, and all investigators who contributed to the Hi-CARAT study. Their collaboration was indispensable in shaping this research. I would also like to extend my appreciation to Prof. Kazushige Ihara at Hirosaki University, for his assistance in coordinating my work schedule, allowing me ample time to focus on completing my doctoral thesis. Moreover, I would like to thank my parents, and grandparents for their enduring love and support throughout my doctoral studies. Your encouragement has been a source of strength during my journey.

Conflicts of interest

Dr. Yokota received research funding from Nihon Medi-Physics and speaker fees from Chugai Pharmaceutical Co. and AstraZeneca, outside the submitted work. Dr. Nishimura received research funding from AstraZeneca KK, Kyorin Pharmaceutical Ltd, and MSD. The data used in this study were obtained from Hi-CARAT study funded by the Ministry of Education, Culture, Sports, Science and Technology of Japan (12877091 to Dr. Nishimura) and a search grant from MSD, AstraZeneca, and Kyorin. The remaining authors have no conflicts of interest to report.

References

Andersen PK and Gill RD (1982) Cox's regression model for counting processes: a large sample study. Ann Stat 10, 1100–1120.

Antalffy T, De Simoni A and Griffiths CJ (2020) Promising peak flow diary compliance with an electronic peak flow meter and linked smartphone app. NPJ Prim Care Respir Med 30, 18–19.

Barnes PJ (2019) Inflammatory endotypes in COPD. Allergy 74, 1249–1256.

Bime C, Wei CY, Holbrook JT, Sockrider MM, Revicki DA and Wise RA (2012) Asthma symptom utility index: reliability, validity, responsiveness, and the minimal important difference in adult asthmatic patients. J Allergy Clin Immunol 130, 1078–1084.

Brightling CE, Monteiro W, Ward R, Parker D, Morgan MDL, Wardlaw AJ and Pavord ID (2000) Sputum eosinophilia and short-term response to prednisolone in chronic obstructive pulmonary disease: a randomised controlled trial. Lancet 356, 1480–1485.

Buckley JP and Richardson DB (2012) Seasonal modification of the association between temperature and adult emergency department visits for asthma: A case-crossover study. Environ Health 11, 1–6.

Castillo JR, Peters SP and Busse WW (2017) Asthma exacerbations: pathogenesis, prevention, and treatment. J Allergy Clin Immunol Pract 5, 918–927.

Cong X, Xu X, Zhang Y, Wang Q, Xu L and Huo X (2017) Temperature drop and the risk of asthma: a systematic review and meta-analysis. Environ Sci Pollut Res Int 24, 22535–22546.

Cox DR (1972) Regression models and life-tables. J. R. Stat. Soc. B 34, 187–202.

Dal Negro RW, Micheletto C, Tognella S, Turati C, Bisato R, Guerriero M, Sandri M and Turco P (2007) PIKO-1, an effective, handy device for the patient's personal PEFR and FEV1 electronic long-term monitoring. Monaldi Arch Chest Dis 67, 84–89.

Dempster AP, Laird NM and Rubin DB (1977) Maximum likelihood from incomplete data via the EM algorithm. J. R. Stat. Soc. B 39, 1–22.

Duvall MG, Krishnamoorthy N and Levy BD (2019) Non-type 2 inflammation in severe asthma is propelled by neutrophil cytoplasts and maintained by defective resolution. Allergol Int 68, 143–149.

Ebmeier S, Thayabaran D, Braithwaite I, Bénamara C, Weatherall M and Beasley R (2017) Trends in international asthma mortality: analysis of data from the WHO Mortality Database from 46 countries (1993-2012). Lancet 390, 935–945.

Engelkes M, Baan EJ, de Ridder MAJ, Svensson E, Prieto-Alhambra D, Lapi F, Giaquinto C, Picelli G, Boudiaf N, Albers F, et al. (2020) Incidence, risk factors and re-exacerbation rate of severe asthma exacerbations in a multinational, multidatabase pediatric cohort study. Pediatr Allergy Immunol 31, 496–505.

Flood-Page P, Swenson C, Faiferman I, Matthews J, Williams M, Brannick L, Robinson D, Wenzel S, Busse W, Hansel TT, et al. (2007) A study to evaluate safety and efficacy of mepolizumab in patients with moderate persistent asthma. Am J Respir Crit Care Med 176, 1062–1071.

Fonseca JA, Costa-Pereira A, Delgado L, Silva LN, Magalhães M, Castel-Branco MG and Vaz M (2005) Pulmonary function electronic monitoring devices: a randomized agreement study. Chest 128, 1258–1265.

Foster P, Rosenberg H, Asquith K and Kumar R (2008) Targeting eosinophils in asthma. Curr Mol Med 8, 585–590.

Frey U, Brodbeck T, Majumdar A, Robin Taylor D, Ian Town G, Silverman M and Suki B (2005) Risk of severe asthma episodes predicted from fluctuation analysis of airway function. Nat 438, 667–670.

Gallagher A, Edwards M, Nair P, Drew S, Vyas A, Sharma R, Marsden PA, Wang R and Evans DJW (2021) Anti-interleukin-13 and anti-interleukin-4 agents versus placebo, anti-interleukin-5 or anti-immunoglobulin-E agents, for people with asthma. Cochrane Database Syst Rev 10.

Garudadri S and Woodruff PG (2018) Targeting Chronic Obstructive Pulmonary Disease Phenotypes, Endotypes, and Biomarkers. Ann Am Thorac Soc 15, S234–S238.

Gönen M and Heller G (2005) Concordance probability and discriminatory power in proportional hazards regression. Biometrika 92, 965–970.

Gour N and Wills-Karp M (2015) IL-4 and IL-13 signaling in allergic airway disease. Cytokine 75, 68–78.

Hammad H and Lambrecht BN (2021) The basic immunology of asthma. Cell 184, 1469–1485.

Hayata A, Matsunaga K, Hirano T, Akamatsu K, Ichikawa T, Minakata Y and Ichinose M (2013) Stratifying a risk for an increased variation of airway caliber among the clinically stable asthma. Allergol Int 62, 343–349.

Honkoop PJ, Taylor DR, Smith AD, Snoeck-Stroband JB and Sont JK (2013) Early detection of asthma exacerbations by using action points in self-management plans. Eur Respir J 41, 53–59.

Hosmer D and Lemeshow S (2013) *Applied Logistic Regression*. (Wiley: New York, NY).

Hudey SN, Ledford DK and Cardet JC (2020) Mechanisms of non-type 2 asthma. Curr Opin Immunol 66, 123–128.

Jackson D, Aljamil N, Roxas C, Fernandes M, Green L, Kavanagh J, D'Ancona G and Kent B (2018) The 'T2-low' asthma phenotype: could it just be T2-high asthma treated with corticosteroids? Thorax 73, A124–A125.

Jensen JLWV (1906) Sur les fonctions convexes et les inégalités entre les valeurs moyennes. Acta. Math. 30, 175–193.
Jian W, Gao Y, Hao C, Wang N, Ai T, Liu C, Xu Y, Kang J, Yang L, Shen H, et al. (2017) Reference values for spirometry in Chinese aged 4-80 years. J Thorac Dis 9, 4538–4549.
Juniper EF, Guyatt GH, Epstein RS, Ferrie PJ, Jaeschke R and Hiller TK (1992) Evaluation of impairment of health related quality of life in asthma: development of a questionnaire for use in clinical trials. Thorax 47, 76–83.
Juniper EF, O'Byrne PM, Guyatt GH, Ferrie PJ and King DR (1999) Development and validation of a questionnaire to measure asthma control. Eur Respir J 14, 902–907.
Kaminsky DA, Bates JHT and Irvin CG (2000) Effects of cool, dry air stimulation on peripheral lung mechanics in asthma. Am J Respir Crit Care Med 162, 179–186.
Kaplan EL and Meier P (1958) Nonparametric estimation from incomplete observations. J Am Stat Assoc 53, 457–481.
Kimura H, Konno S, Nakamaru Y, Makita H, Taniguchi N, Shimizu K, Suzuki M, Ono J, Ohta S, Izuhara K, et al. (2017) Sinus computed tomographic findings in adult smokers and nonsmokers with asthma. Analysis of clinical Indices and biomarkers. Ann Am Thorac Soc 14, 332–341.
Kimura H, Konno S, Makita H, Taniguchi N, Shimizu K, Suzuki M, Kimura H, Goudarzi H, Nakamaru Y, Ono J, et al. (2018) Prospective predictors of exacerbation status in severe asthma over a 3-year follow-up. Clin Exp Allergy 48, 1137–1146.
Kimura Hirokazu, Konno S, Makita H, Taniguchi N, Kimura Hiroki, Goudarzi H, Shimizu K, Suzuki M, Shijubo N, Shigehara K, et al. (2018) Serum periostin is associated with body mass index and allergic rhinitis in healthy and asthmatic subjects. Allergol Int 67, 357–363.
Kimura Hirokazu, Makita H, Taniguchi N, Takei N, Matsumoto M, Kimura Hiroki, Goudarzi H, Shimizu K, Suzuki M, Nishimura M, et al. (2021) Determination of the cutoff values of Th2 markers for the prediction of future exacerbation in severe asthma: An analysis from the Hokkaido Severe Asthma Cohort Study. Allergol Int 70, 68–73.
Leander J, Jirstrand M, Eriksson UG and Palmér R (2021) A stochastic mixed effects model to assess treatment effects and fluctuations in home‐measured peak expiratory flow and the association with exacerbation risk in asthma. CPT Pharmacometrics Syst Pharmacol 11, 212.
Li J, Lin LH, Wang J, Peng X, Dai HR, Xiao H, Li F, Wang YP, Yang ZJ and Li L (2014) Interleukin-4 and interleukin-13 pathway genetics affect disease susceptibility, serum immunoglobulin E levels, and gene expression in asthma. Ann Allergy Asthma Immunol 113, 173-179.e1.
Lin H, Turnbull BW, McCulloch CE and Slate EH (2002) Latent class models for joint analysis of longitudinal biomarker and event process data. J Am Stat Assoc 97, 53–65.

Liu DC and Nocedal J (1989) On the limited memory BFGS method for large scale optimization. Math Program 45, 503–528.
Lommatzsch M and Virchow JC (2014) Severe asthma: definition, diagnosis and treatment. Dtsch Arztebl Int 111, 847–855.
Lopez AF, Begley CG, Williamson DJ, Warren DJ, Vadas MA and Sanderson CJ (1986) Murine eosinophil differentiation factor. An eosinophil-specific colony-stimulating factor with activity for human cells. J Exp Med 163, 1085–1099.
Murugesan N, Saxena D, Dileep A, Adrish M and Hanania NA (2023) Update on the role of FeNO in asthma management. Diagnostics (Basel) 13.
Natarajan S, Castner J and Titus AH (2016) Smart phone-based peak expiratory flow meter. Electron Lett 52, 904–905.
Pijnenburg MW (2019) The role of FeNO in predicting asthma. Front Pediatr 7.
Pizzichini E, Pizzichini MMM, Gibson P, Parameswaran K, Gleich GJ, Berman L, Dolovich J and Hargreave FE (1998) Sputum eosinophilia predicts benefit from prednisone in smokers with chronic obstructive bronchitis. Am J Respir Crit Care Med 158, 1511–1517.
R Development Core Team (2019) R: A language and environment for statistical computing.
Revicki DA, Leidy NK, Brennan-Diemer F, Sorensen S and Togias A (1998) Integrating patient preferences into health outcomes assessment: the multiattribute Asthma Symptom Utility Index. Chest 114, 998–1007.
Ruopp MD, Perkins NJ, Whitcomb BW and Schisterman EF (2008) Youden index and optimal cut-point estimated from observations affected by a lower limit of detection. Biom J 50, 419–430.
Schoettler N and Strek ME (2020) Recent advances in severe asthma: from phenotypes to personalized medicine. Chest 157, 516–528.
Siva R, Green RH, Brightling CE, Shelley M, Hargadon B, McKenna S, Monteiro W, Berry M, Parker D, Wardlaw AJ, et al. (2007) Eosinophilic airway inflammation and exacerbations of COPD: a randomised controlled trial. Eur Respir J 29, 906–913.
Sun S, Jin Y, Chen C, Sun B, Cao Z, Lo IL, Zhao Q, Zheng J, Shi Y and Zhang XD (2018) Entropy change of biological dynamics in asthmatic patients and its diagnostic value in individualized treatment: a systematic review. Entropy (Basel) 20.
Thamrin C, Taylor DR, Jones SL, Suki B and Frey U (2010) Variability of lung function predicts loss of asthma control following withdrawal of inhaled corticosteroid treatment. Thorax 65, 403–408.
Thamrin C, Nydegger R, Stern G, Chanez P, Wenzel SE, Watt RA, FitzPatrick S, Taylor DR and Frey U (2011) Associations between fluctuations in lung function and asthma control in two populations with differing asthma severity. Thorax 66, 1036–1042.

Thomas MS, Parolia A, Kundabala M and Vikram M (2010) Asthma and oral health: a review. Aust Dent J 55, 128–133.
Tibshirani R (1996) Regression shrinkage and selection via the Lasso. J R Stat Soc Series B Stat Methodol 58, 267–288.
Tiotiu AI, Novakova P, Nedeva D, Chong-Neto HJ, Novakova S, Steiropoulos P and Kowal K (2020) Impact of air pollution on asthma outcomes. Int J Environ Res Public Health 17, 1–29.
Verschelden P, Cartier A, L'Archevêque J, Trudeau C and Malo JL (1996) Compliance with and accuracy of daily self-assessment of peak expiratory flows (PEF) in asthmatic subjects over a three month period. Eur Respir J 9, 880–885.
Wenzel SE, Fahy J V., Irvin C, Peters SP, Spector S, Szefler SJ, Casale TB, Cloutier MM, Elias JA, Liu MC, et al. (2000) Proceedings of the ATS workshop on refractory asthma: current understanding, recommendations, and unanswered questions. American Thoracic Society. Am J Respir Crit Care Med 162, 2341–2351.
Wulfsohn MS and Tsiatis AA (1997) A joint model for survival and longitudinal data measured with error. Biometrics 53, 330.